ROYAL SOCIETY OF CHEMISTRY

PAPER

Check for updates

Repurposed marble dust as a promising adsorbent for modelling the removal of methylene blue from aqueous solutions†

Ankita Sharma, [ID] [a] Subrata Panda, [ID] [b] Sudesh Kumar [ID] [ac] and Yogesh Chandra Sharma [ID] *[d]

Marble dust (MD) is a significant landfill waste generated as a byproduct of mining and construction industries. Methylene blue (MB) is a widely used hazardous dye responsible for serious ecological and health risks, and its treatment has become increasingly alarming. This investigation scrutinizes the facile preparation of a non-complex, low-cost, sustainable, and industrially feasible adsorbent along with conducting its mechanistic studies, including XRD, TEM, WD-XRF, FE-SEM, FTIR, BET, TGA, and XPS, followed by its implementation in the removal of MB dye. To examine the relative influence of different variables, namely, time, temperature, pH, activated marble dust (AMD) amount and MB concentration, a central composite design (CCD) model of response surface methodology (RSM) was employed with approved $R^2 = 0.9914$, supporting the credibility of the model. The additional verification was provided by ANOVA results, including the lack of fit and p-values, endorsing a quadratic model. The 3D response plots clarified the influence of variables on the removal yield; the pH had a dominant influence on the system at its higher value, while at lower pH values, the concentration played a more significant role. The removal process followed a pseudo-second-order kinetics ($R^2 = 0.999$) and adhered to the Langmuir isotherm model ($R^2 = 0.9735$), representing monolayer adsorption with $q_{max} = 1.16$ mg g^{-1}. The thermodynamic study of the process fell under Henry's law region and unveiled that the removal of MB is exothermic, spontaneous, and feasible and has appreciable reproducibility up to five cycles. The overall process of adsorption followed physisorption, which was confirmed by the adhesion probability and activation energy calculations. The adsorption process followed pore diffusion and bond formation mechanisms.

Sustainability spotlight

Methylene blue, a substantially utilized dye, often discharged into aquatic ecosystems without adequate treatment, causes significant ecological and health hazards. Concurrently, waste marble dust from the marble industries contributes significantly to landfill accumulation. This research innovatively repurposes waste marble dust as a cost-effective and sustainable adsorbent for the treatment of methylene blue in wastewater. The research reveals a remarkable removal efficiency under normal conditions, accompanied by impressive reusability, thereby maximizing the viability of marble dust. Besides addressing critical ecological concerns, this study aligns seamlessly with the United Nations Sustainable Development Goals (SDGs), particularly SDG 6 (Clean water and sanitation), SDG 12 (Responsible consumption and production), and SDG 14 (Life below water).

1 Introduction

Marble dust is one of the hazardous air and soil landfill pollutants produced majorly in India, Egypt, China, Italy, and Spain, with an annual average production of 1 million tons. Marble dust is produced as waste in construction industries during quarrying, cutting, and polishing stages.[1,2] The International Agency for Research on Cancer (IARC) 1997 classified marble dust as a carcinogenic substance responsible for lung cancer and bronchitis in marble workers. The alteration in the rate of photosynthesis and transpiration and adverse effects on plant growth were also observed.[3] Dyes are complex, colored

[a]Department of Chemistry, Banasthali Vidyapith, Banasthali 304022, India

[b]Department of Ceramic Engineering, Indian Institute of Technology (Banaras Hindu University), Varanasi 221005, India

[c]Department of Chemistry, National Institute of Education, National Council of Education Research and Training, New Delhi 110016, India

[d]Department of Chemistry, Indian Institute of Technology (Banaras Hindu University), Varanasi 221005, India. E-mail: ysharma.apc@itbhu.ac.in; Fax: +91 542 6702876; Tel: +91 6702865

Paper

aromatic compounds with large molecular sizes, which give permanent color to the substrate and withstand fading even after exposure to light, water, microbial organisms and oxidizing agents. These benefits are advantageous across many industries, including textile, rubber, pharmaceutics, paper, and plastics.[4] Dyes are possibly the exclusive pollutant that can be detected in water even at minimal levels with the naked eye. Dyes must be eliminated from the effluent prior to discharge into the water bodies since it obstructs the entry of sunlight and inhibits photosynthesis. Moreover, color elevates the chemical oxygen demand (COD) and biological oxygen demand (BOD) and tends to chelate metal ions, leading to microtoxicity in aquatic organisms and decreasing the availability of essential metals.[5] MB is a commonly used cationic ($C_{16}H_{18}N_3SC_1$) thiazine dye with λ_{max} at 663 nm. It forms a stable deep blue color in aqueous solution and a red color in benzene.[6] It was identified as an antidote for carbon monoxide and cyanide and is used as a redox indicator in laboratories.[7,8] It has been reported that MB exceeding 7 mg kg^{-1} in water could lead to diseases like methemoglobinemia through direct oxidation, while its dosage above 15 mg kg^{-1} can result in hemolysis.[9]

There are numerous methods for the elimination of dyes, *viz.* adsorption, oxidation, filtration, coagulation–flocculation, and photodegradation.[10–14] The drawbacks associated with most of these processes are the generation of enormous sludge, expensive, ineffective elimination of dyes, high demand for chemicals, *etc.* The generation of sludge and its tedious management requires a lucid method. Furthermore, most dyes exhibit stability against both photodegradation and biodegradation, thereby leading to their improper removal. In the sight of these consequences, the interest of researchers has shifted to the adsorption method, which is a simple, cost-effective method with high treatment efficiency without generating hazardous compounds.[15,16] However, the challenge with adsorption technology is the selection of effective and inexpensive adsorbent materials. Nowadays, such adsorbents are widely available and easy to synthesize from waste materials like coal,[17] sand,[18,19] marble dust,[20] and biochar made from various biomass materials,[21] reducing the waste besides water treatment.[22]

The RSM technique is a statistical modelling technique with two popular designs, *i.e.*, Box-Behnken Design (BBD) and Central Composite Design (CCD). The BBD is an effective design that requires a few runs. They have statistical characteristics like rotatability or near-rotatability. The BBD does not have center points while the CCD is a factorial design with center points that expand the cuboidal area of the original factorial design. The advantage of having these center points is that they provide an analysis of the curvature of the response over different factor levels.[23]

This study deals with a facile and inexpensive nanoadsorbent synthesized from waste marble dust. The vitality of the nanoadsorbent was explored for MB dye with the utilization of RSM-FCCCD (Face Centered Central Composite Design) to examine the interaction among independent variables like time, temperature, pH, initial MB concentration. The best-optimized conditions with DF = 1 (Desirability Factor) suggested by the model were experimentally approved. To understand the detailed mechanisms, kinetic, isotherm, and thermodynamic studies were performed along with XPS studies. This research explores the scope of sustainable water treatment using a novel nanoadsorbent fabricated using facile techniques rather than employing raw or composite adsorbents synthesized from metallurgical waste.

2 Experimentation

2.1 Materials

The chemicals employed to carry out the experiments were of analytical grade. The methylene blue dye (mol. wt 319.85 g mol^{-1}) was used to prepare the stock solution of 250 mg L^{-1} by solubilizing 0.25 g powder of MB in 1 L distilled water. The NaOH (mol. wt 40 mg L^{-1}) pellets and HCl (mol. wt 36.46 mg L^{-1}) of Molychem and Emparta ACS of 98% and 37% purity were used to make a 0.1 M solution of each to maintain the requisite pH. NaCl (mol. wt 58.44) of 99.5% purity from Fischer Scientific was used to perform the spH$_{zpc}$ experiments of AMD.

2.2 Experimental procedure

The particle size of marble dust was reduced by mechanical pulverization followed by annealing. The schematic in Fig. 1 gives an outlook of the experimental process followed. The Section S1.1 of the ESI file† gives a detailed account of the experimental procedure.

The experimental variables like pH, adsorbent dose, and initial MB concentration were determined according to the experimental runs outlined in Table 3. The percentage removal of MB and (q_e) adsorption capacity were estimated using eqn (1) and (2), respectively.

$$\% \text{ removal of } MB = \frac{C_i - C_f}{C_i} \times 100 \qquad (1)$$

$$q_e = \frac{(C_i - C_e)}{W} \times V \qquad (2)$$

C_i (mg L^{-1}) is the initial concentration of MB solutions, C_f (mg L^{-1}) is the final concentration of MB solutions and C_e (mg L^{-1}) is the equilibrium concentration of MB solutions, W (g) is the AMD dose and V (mL) is the volume of MB solution.

2.3 Characterization techniques

A wavelength-dispersive X-ray fluorescence spectrometer (Malvern Panalytical Zetium) was used for elemental analysis. For the batch top X-ray diffraction system (Rigaku Miniflex 600 Desktop), the range of 2θ was between 10°–70° with a scanning rate of 2° min^{-1} equipped with a copper laser source (Cu Kα at λ = 1.54 Å) at 5 mA and 20 kV. The X-ray diffraction data was analyzed by X'Pert HighScore Version 2.2 (2.2.0). Scanning electron microscope (Nova Nano SEM 450) was employed for the surface morphology study. Samples were coated with gold before charging for effective imaging. Fourier transform infrared spectroscopy (ThermoElectron Scientific Instruments LLC Nicolet iS5) was employed to determine and distinguish the bonding and functional groups. The surface area analyzer
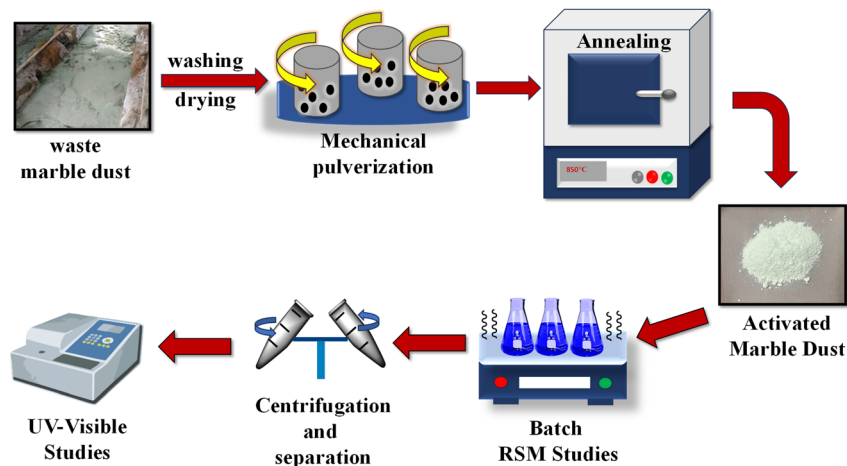
Fig. 1 Schematic of the experimental procedure.

(Quantachrome) was used for surface area studies. The X-ray photoelectron spectroscopy (XPS) was performed using Thermo Fisher Scientific (K-Alpha Model). The final remaining concentration after adsorption was measured using a UV-spectrophotometer (Shimadzu UV-1800). The thermo scientific pH meter (Orion Star A211) was used to estimate the pH. Some other instruments, such as a water bath shaker (Remi RSB-12), centrifugation machine (Remi PR-24), hot air oven (Remi RDHO 80), and muffle furnace, were also used during experiments.

2.4 Design of experiments (DoE)

The design of experiments (DoE) is an effective statistical technique that deals with designing, executing, analyzing and assessing the controlled tests to determine the variables that influence the value of response used to understand the relation between variables influencing a process and its response.[24] The DoE includes scheming experiments and examining the data with statistical techniques.

3 Results and discussion

3.1 Adsorbent characterization

X-ray diffraction (XRD) from 10° to 70° range was performed for MD and Activated Marble Dust (AMD) as displayed in Fig. 2(a) and (b), respectively. The MD (washed and dried) has calcite and AMD has lime as a major component. The peaks at 30.1°, 31.3°, 35.7°, 39.3°, 43.1°, 47.5°, 48.6°, and 50.4° correspond to calcite (JCPDS No. 05-0586) with *hkl* values (104), (006), (110), (113), (202), (018), (116), respectively.[25] After calcination at 8323 K, CO_2 is removed and CaO is formed, which shows peaks at 31.8°, 37.1°, 53.6°, 64°, and 67.2° corresponding to lime (JCPDS No. 82-1691). The *hkl* values for the corresponding peaks are (110), (200), (220), (311), and (222), respectively.[25] The sharp peaks show that both samples are highly crystalline.

For the wavelength dispersive X-ray fluorescence (WD-XRF) analysis, the sample was prepared by the fused bead technique by adding lithium tetraborate as a fluxing agent and lithium iodide as a releasing agent. The XRF data of marble dust is

provided in Table 1. The major component is CaO (92.7%), accompanied by MgO and SiO_2 at 3.58% and 2.11%, respectively. The other metals are present in the form of oxides like Al_2O_3, Fe_2O_3, P_2O_5, Na_2O, and K_2O, which are present in low proportions.

The FTIR is scanned from 500–4000 cm^{-1} using KBr pellets. Fig. 3 shows the graph plotted between % transmittance and wavenumber for MD and AMD. From the plot of MD [Fig. 3(a)], various vibrations of CO_3^{2-} were observed from 712 to 2984 cm^{-1}, confirming the presence of $CaCO_3$. The peaks at 712, 876, and 1443 cm^{-1} are due to the in-plane bending, out-of-plane bending and asymmetric stretching of C–O of CO_3^{2-}, respectively, with the peak at 1799 cm^{-1} appearing due to the combination of symmetric and in-plane bending of carbonate.[26] The peaks around 2515, 2874, and 2984 cm^{-1} are due to the presence of calcite and vibrations due to the C–H bond showing the presence of some volatile compounds confirmed by their disappearance after calcination.[27–29] The peaks due to symmetric O–H vibration due to environmental moisture in CaO were observed at 1635, 3438 and 3652 cm^{-1}. For AMD
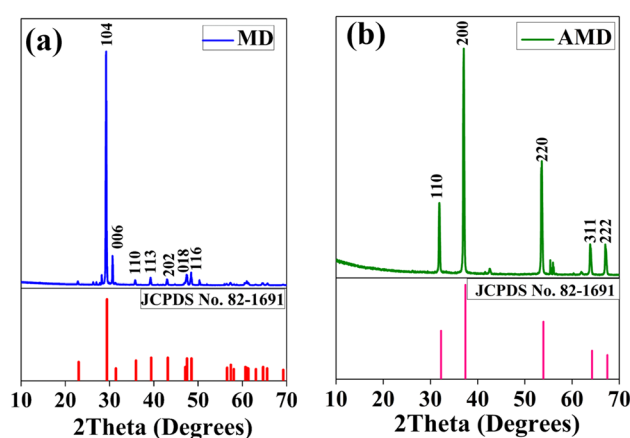

Fig. 2 XRD plot with *hkl* values of corresponding peaks for (a) MD (b) AMD.

Table 1 Wavelength dispersive X-ray fluorescence elemental analysis of AMD adsorbent for MB removal

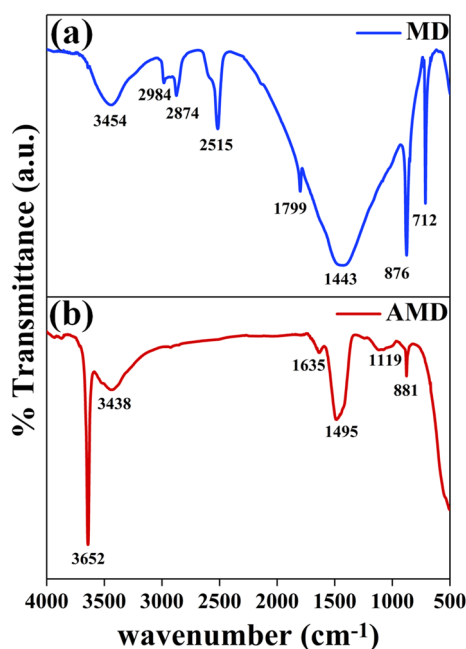| Compound	Value	Unit
CaO	92.74	%
MgO	3.58	%
SiO_2	2.11	%
Al_2O_3	0.525	%
Fe_2O_3	0.371	%
P_2O_5	0.169	%
SO_3	0.142	%
Na_2O	0.107	%
K_2O	0.102	%
Cr_2O_3	162.3	ppm
MnO	297.7	ppm
Cl	363	ppm
ZnO	60.4	ppm

Fig. 3 FTIR plot of (a) MD and (b) AMD.

[Fig. 3(b)], peaks at 881 cm^{-1} and 1495 cm^{-1} are because of the Ca–O bond vibration of CaO.[30]

The FE-SEM (Field Emission Scanning Electron Microscopy) images of adsorbent AMD show that the surface is rough and has a non-uniform morphology [Fig. 4(a)]. The rough surface of AMD is an advantage because it provides more surface for adsorption. It can be observed from Fig. 4(b) that the surface has some crystals that show its hydration due to environmental moisture and lead to $Ca(OH)_2$ formation. The CaO is highly hygroscopic, so it reacts with moisture and forms $Ca(OH)_2$.[26] The amount of the $Ca(OH)_2$ phase is very low; thus, it was not visible in XRD data. Fig. 4(c) displays the TEM (Transmission Electron Microscopy) image of the irregular-shaped AMD particles and the plot in Fig. 4(d) demonstrates the average particle diameter of 15.8 nm of AMD particles. The SAED

(Selected Area Electron Diffraction) analysis [Fig. 4(e)] shows the CaO and $Ca(OH)_2$ phases.

To predict the calcination temperature of MD, TGA (thermogravimetric analysis) was performed from room temperature to 1273 K, as represented in Fig. 5(a). It can be noted that the percentage weight loss is 0.23% between 581 K and 1006 K because of the evaporation of surface water left after drying. A sudden major weight loss of 6.76% was observed between 1016 K and 1153 K due to the release of CO_2 from $CaCO_3$. Thus, the calcined temperature was chosen as 1123 K.[24] To confirm the complete removal of CO_2 after calcination, the AMD powder was tested by adding it to HCl; the absence of effervescence indicated no residual CO_2.

To investigate the surface area of the adsorbent, the N_2 gas was adsorbed for BET (Brunauer–Emmett–Teller) analysis of AMD. A graph between the relative pressure and volume was plotted, which shows the adsorption and desorption data of AMD, as shown in Fig. 5(b). The IUPAC (International Union of Pure and Applied Chemistry) has categorized various types of adsorption isotherms, out of which AMD follows the type IV of isotherms showing mesoporous surfaces. The AMD has a 16.77 nm average pore size and 0.07 cc g^{-1} (pore radius below 109.66 nm at $P/P_0 = 0.991$) total pore volume. It has 15.895 m^2 g^{-1} and 8.423 m^2 g^{-1} surface area (Langmuir and multipoint BET, respectively). These parameters reveal that the adsorbent has good adsorbent properties, such as high surface area.

A 0.01 M NaCl solution was used for the measurement of pH_{zpc} (point of zero charge) of the adsorbent AMD. 0.01 M NaCl solution of 50 mL was taken in each reagent bottle. The pH was adjusted from 2 to 12 for 0.1 M each of NaOH and HCl and 0.2 g of AMD was added. The bottles were kept in a water bath shaker for 48 h isothermally at 298 ± 3 K. The final pH was determined and a graph was plotted between ΔpH ($pH_{final} - pH_{initial}$) and initial pH. The point where the ΔpH value intersects the x-axis gives the value of pH_{zpc}.[18] The pH_{zpc} for AMD was observed at 12 [Fig. 5(c)], indicating that the surface of AMD is neutral at this pH, containing neutral species of CaO, i.e., (Ca–OH).[29] In addition, the surface is positively charged below this point and negatively charged above this. At lower pH, CaO receives proton from the medium and forms $Ca–OH^{2+}$ species, and at pH above 12, it exists as (Ca–O) on deprotonation.

3.2 Model fitting of MB by CCD statistical analysis

All experiments were designed using Design Expert 13 software in which correlation among various independent variables and responses is established. In this instance, the face-centered central composite design was utilized to model the experiments. Independent process variables like time, pH, AMD dose, initial concentration of MB, and temperature were used with three levels (Table 2). Here, while finalizing the range of pH, the pH_{zpc} was taken into consideration.

A relationship between the process variables (pH, time, temperature etc.) and the output response (percentage removal) was drawn using a quadratic model. Table 3 shows the experimental and predicted values of the percentage of MB removal derived from the model.
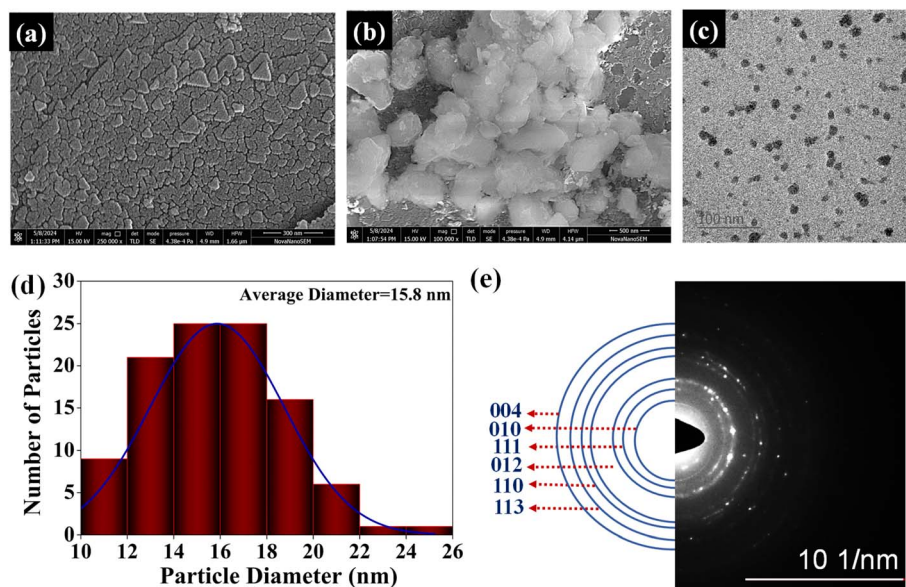
Fig. 4 FE-SEM images of AMD (a) AMD surface (b) Ca(OH)$_2$ crystals on the AMD surface (c) TEM image of AMD particles (d) AMD particle diameter plot (e) SAED pattern of AMD.
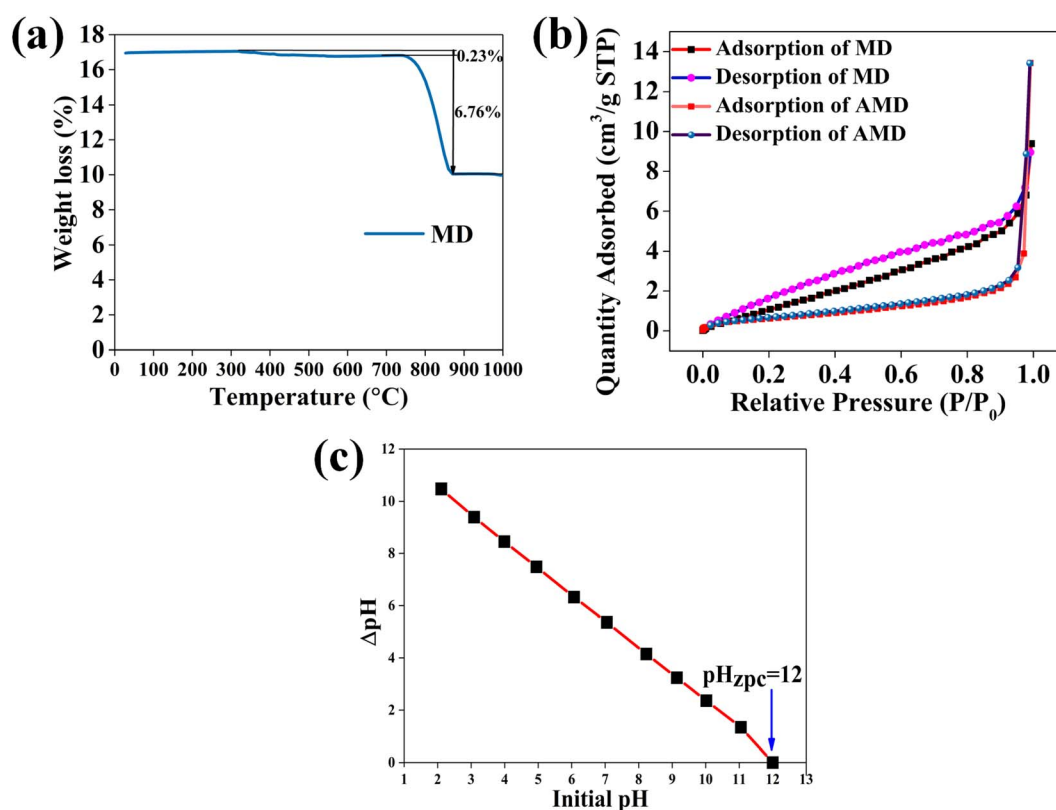

Fig. 5 (a) TGA plot of MD indicating a major weight loss of 6.76% around 1123 K (b) N$_2$ adsorption BET plot of AMD used for MB removal (type IV isotherm) (c) pH$_{zpc}$ plot of the adsorbent AMD for the removal of MB (pH$_{zpc}$ = 12) [0.01 M NaCl from 2 to 12 pH with 0.2 g of AMD for 48 hours at room temperature].

The quadratic expression obtained by the ANOVA (analysis of variance) approach is given below in eqn (3). Here, percentage dye removal is the percentage of MB removed by AMD; A is the pH of the system, B (mg L^{-1}) is the initial MB concentration, C (g L^{-1}) is AMD dose, D (minute) is time and E (K) is the temperature. In the below quadratic equation, the positive or negative sign before the

Paper

Table 2 List of independent design variables and their experimental ranges for the removal of MB dye

Variables	Notation	Unit	Range −1	0	+1
pH	A		4	9	14
Initial concentration	B	mg L^{-1}	10	30	50
AMD dose	C	g	0.1	0.55	1
Time	D	minute	30	135	240
Temperature	E	K	303	313	323

coefficient shows the nature of the influence of that individual variable on the model response, while the magnitude of the coefficient indicates its extent of influence on the response.

$$\begin{aligned}
\text{Percentage dye removal} &= 58.3916 + 0.87 \times A - 11.26 \\
&\times B + 4.09 \times C - 5.82 \times D + 2.48 \times E + 2.99 \\
&\times AB - 0.59 \times AC - 8.66 \times AD + 4.29 \times AE \\
&- 0.24 \times BC + 2.43 \times BD + 0.01 \times BE + 1.27 \\
&\times CD + 2.30 \times CE + 3.07 \times DE - 18.03 \\
&\times A^2 + 21.42 \times B^2 - 16.43 \times C^2 + 22.37 \\
&\times D^2 - 7.16 \times E^2
\end{aligned} \quad (3)$$

Table 4 outlines the results of ANOVA for the quadratic model level response. The ANOVA applied for the removal of MB with AMD showed a substantial model significance with an F-value of 131.80. The p-values below 0.0001 indicate that model terms, *i.e.*, quadratic terms (A^2, B^2, C^2, E^2), interaction terms (AB, CE), and linear terms (A, B, C, D, E) are justified. The lack of fit F-value 22.93 indicates the proposed model is well fitted to the

Table 3 List of CCD experimental runs with independent variables and responses for MB

Std	Run	pH	Initial conc. (mg L^{-1})	Adsorbent dose (g)	Time (min)	Temp. (K)	Dye removal (%)
21	1	4	10	1	30	323	23.91
15	2	4	50	1	240	303	46.45
14	3	14	10	1	240	303	88.7
34	4	14	30	0.55	135	313	83.73
20	5	14	50	0.1	30	323	54.14
25	6	4	10	0.1	240	323	51.88
6	7	14	10	1	30	303	91.48
40	8	9	30	0.55	240	313	55.14
22	9	14	10	1	30	323	59.57
37	10	9	30	0.1	135	313	49.84
2	11	14	10	0.1	30	303	95.81
12	12	14	50	0.1	240	303	80.36
43	13	9	30	0.55	135	313	54.57
9	14	4	10	0.1	240	303	52.47
17	15	4	10	0.1	30	323	36.94
8	16	14	50	1	30	303	70.66
31	17	4	50	1	240	323	31.30
27	18	4	50	0.1	240	323	50.07
11	19	4	50	0.1	240	303	54.14
3	20	4	50	0.1	30	303	42.67
35	21	9	10	0.55	135	313	50.95
23	22	4	50	1	30	323	21.77
7	23	4	50	1	30	303	43.76
29	24	4	10	1	240	323	29.35
33	25	4	30	0.55	135	313	51.48
18	26	14	10	0.1	30	323	74.53
32	27	14	50	1	240	323	45.83
16	28	14	50	1	240	303	72.74
10	29	14	10	0.1	240	303	96.76
4	30	14	50	0.1	30	303	74.5
19	31	4	50	0.1	30	323	31.30
1	32	4	10	0.1	30	303	51.88
44	33	9	30	0.55	135	313	50.27
13	34	4	10	1	240	303	58.27
26	35	14	10	0.1	240	323	86.8
38	36	9	30	1	135	313	38.20
30	37	14	10	1	240	323	62.9
24	38	14	50	1	30	323	40.65
42	39	9	30	0.55	135	323	55.17
41	40	9	30	0.55	135	303	72.30
39	41	9	30	0.55	30	313	46.92
5	42	4	10	1	30	303	43.69
36	43	9	50	0.55	135	313	38.27
28	44	14	50	0.1	240	323	66.04

Table 4 ANOVA for RSM CCD quadratic model for adsorption of MB dye with AMD

Source	Sum of squares	df	Mean square	F-Value	p-Value	
Model	15 666.62	20	783.33	118.55	<0.0001	Significant
A-pH	8071.45	1	8071.45	1221.54	<0.0001	
B-Initial conc.	1074.79	1	1074.79	162.66	<0.0001	
C-Adsorbent dose	962.30	1	962.30	145.63	<0.0001	
D-Time	459.74	1	459.74	69.58	<0.0001	
E-Temp.	2908.82	1	2908.82	440.22	<0.0001	
AB	486.02	1	486.02	73.55	<0.0001	
AC	17.35	1	17.35	2.63	0.1187	
AD	48.02	1	48.02	7.27	0.0129	
AE	126.84	1	126.84	19.20	0.0002	
BC	2.62	1	2.62	0.3970	0.5349	
BD	10.30	1	10.30	1.56	0.2243	
BE	2.54	1	2.54	0.3839	0.5416	
CD	42.09	1	42.09	6.37	0.0190	
CE	335.29	1	335.29	50.74	<0.0001	
DE	65.89	1	65.89	9.97	0.0044	
A^2	496.75	1	496.75	75.18	<0.0001	
B^2	189.73	1	189.73	28.71	<0.0001	
C^2	215.94	1	215.94	32.68	<0.0001	
D^2	13.71	1	13.71	2.08	0.1632	
E^2	263.28	1	263.28	39.85	<0.0001	
Residual	151.98	23	6.61			
Lack of fit	142.72	22	6.49	0.7006	0.7551	Not significant
Pure error	9.26	1	9.26			
Cor total	15 818.60	43				

experimental results according to the lack of fit. The lack of fit is non-significant based on pure error that shows a good fit. The predicted R^2 value of 0.9665 is closely related to the adjusted R^2 = 0.9838 *viz.* difference is below 0.2, showing decent agreement for the quadratic model. Adequate precision is a proportion of signal-to-noise ratio, which is preferable when its value is higher than 4. For this model, the ratio is 42.228, which signifies an adequate signal. Thus, this model is acceptable for further investigation of the process parameters.

The value of R^2 for this model is 0.9914, which shows that the model has a 99.14% potential to anticipate the variation in response and 0.86% of which cannot be explained by it. The plot of the predicted *versus* actual MB removal percentage (displayed in Fig. S1 of ESI file†) depicts that the cluster of predicted and actual data points align closely around 45° line showing strong correlation between the predicted and actual values. In addition, this indicates that the regression model has potently predicted the removal efficiencies. This plot exhibits a well-built alignment, indicating a robust fit.

Fig. 6 shows the 3D response plots of MB removal, which provide insight into the interaction between different variables. Fig. 6(a) demonstrates the interaction of pH and initial MB concentration. The percentage removal of MB rises with increasing initial MB concentration up to 30 mg L^{-1} and drops on further increasing the concentration. The middle value of the dye concentration, *i.e.*, 30 mg L^{-1}, is advantageous in promoting the combination of adsorption sites and MB molecules to enhance the dye removal at lower pH. On increasing the initial MB concentration, more MB molecules are freely available to interact with the adsorption sites of the adsorbent,

which act as the driving force for the adsorption of MB on AMD to some extent. Furthermore, the increasing initial concentration of MB can create a concentration gradient between the AMD surface and solution, which facilitates the movement of MB molecules on the AMD surface from the solution, promoting the removal.[31] The higher pH significantly favors the percentage removal of MB from 53.18% to 83.60%. Conversely, at low pH (pH = 4), the percentage removal is maximum around 50%. The pH$_{zpc}$ value of the AMD was determined at 12, which indicates that the surface charge of AMD is zero at this value. Moreover, below this point, the AMD surface charge is positive and negative above this point. In this context, the electrostatic interactions play a crucial role. Since MB exists as a cationic dye, it gets repelled from the AMD surface at low pH due to electrostatic repulsion. Additionally, when the pH increases, the AMD surface becomes negatively charged, which attracts the MB dye molecules and promotes their interaction with active sites.[32] It could be observed that the pH wields a dominant influence on the system at higher pH values, while at lower pH values, the concentration plays a more significant role.

As displayed in Fig. 6(b), the dye removal percentage increases, followed by a decrease, *i.e.*, from 75.24% to 83.73% and then decreases to 75.85% with a rise in AMD dose at pH = 14. The increase in AMD dose provides a large number of unsaturated adsorption sites for MB molecules, thereby increasing their removal. At high AMD doses, the interparticle interactions become increasingly prominent and reduce the effective surface area for adsorption. These interactions lead to blockage of adsorption sites by adjacent adsorbent particles, thereby increasing the diffusional resistance and consequently
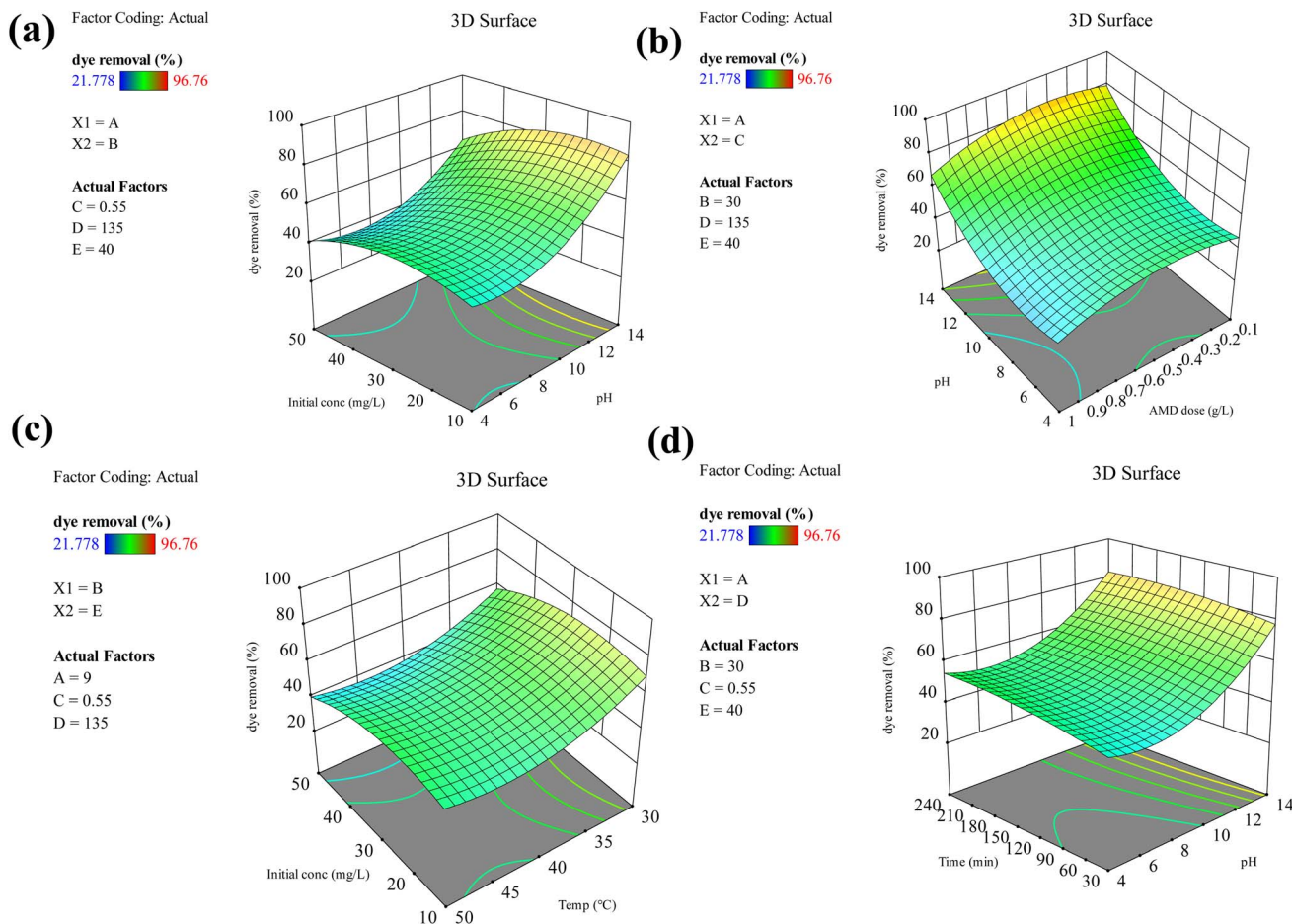
Fig. 6 3D plots demonstrating interactions between (a) pH and initial MB concentration (b) AMD dose and pH (c) temperature and initial MB concentration (d) time and pH.

decreasing the percentage MB removal.[33] The increase in temperature initially increases the yield in Fig. 6(c) because the kinetic energy increases in the system, which augments molecular motion. This rise in thermal energy heightens the frequency of collision between the adsorption sites of AMD and MB molecules, thereby improving MB removal.[34] It could also be due to the activation of additional adsorption sites of the AMD, thereby increasing the adsorbate–adsorbent interactions, leading to a rise in yield.[35] However, further rise in temperature from 313 K to 323 K subside the MB removal because the adsorbed dye molecules gain sufficient energy and desorb from the AMD surface. The influence of time is shown in Fig. 6(d). The increase in contact time from 30 min to 240 min increases the percentage removal of MB, *i.e.*, at pH 9, the adsorption increases from 46.92% to 55.14%, while the longer duration of 240 min gives more time for the interaction between MB molecules and adsorption sites.

3.3 Optimization of desirability factor

The optimization could be achieved by understanding the combined effect of the actual *versus* predicted value plots, 3D plots, and DF. For a high value of DF (DF = 1), the optimized conditions operating adsorption in a conducive direction were

when experiments were performed for 240 min at 303 K for 0.1 g AMD dose at 10 mg L^{-1} initial MB concentration at pH 14. For the above conditions, the predicted MB adsorption was maximum at a removal percentage of 98.39%, while a removal of 96.76% was obtained experimentally. Considering that the pH of water is nearly 7, the optimized condition with DF = 1 at pH 6 was taken into account. The conditions followed were a pH of 6 at an initial MB concentration of 10 mg L^{-1} with 1 g AMD dose at 323 K for 240 minutes. The theoretical removal percentage was 84.11%, while the experimental value obtained was 85.31%.

3.4 Adsorption kinetics

To investigate the influence of time on the removal percentage of MB by AMD, batch experiments of adsorption were performed with 10 mg L^{-1} initial MB concentration and fixed adsorbent dose of 1 g at 313 K at pH 6 for 30–270 min with 30 min time interval. Aliquots of supernatant of the sample were collected from the centrifuge tubes after requisite time interval for analysis of residual MB concentration. The pseudo-first order, pseudo-second order, intraparticle, Boyd and Elovich models were linearly fitted separately for empirical data to elaborate the kinetics of MB on AMD surface. The pseudo-first order linear equation can be represented as (eqn (4)):

$$\ln(q_e - q_t) = \ln q_e - k_1 t \tag{4}$$

Here, q_e and q_t (mg g^{-1}) are the amounts of MB adsorbed at equilibrium and at time t, and the k_1 (min^{-1}) is a pseudo-first-order rate constant. A linear plot between $\ln(q_e - q_t)$ and t following eqn (2) is displayed in Fig. 7(a). Generally, based on R^2, *i.e.*, the value of the correlation coefficient, the optimal fit is selected, which should be close to unity.[36] The R^2 obtained is 0.9303, which implies that the empirical data considerably fitted the pseudo-first-order model.

The pseudo-second-order equation determines the rate of adsorption by squaring vacant adsorption sites on the surface. This model considers that the adsorption process is governed by chemical forces, which transport or share electrons between the adsorbate and adsorbent.[37] It is explained as shown in eqn (5). On integrating for the same boundary conditions, it was applied in this study to explain the kinetics of the empirical data using the linear equation as (eqn (6)):

$$\frac{dq_t}{dt} = k_2(q_e - q_t)^2 \tag{5}$$

$$\frac{t}{q_t} = \frac{1}{k_2 q_e^2} + \frac{t}{q_e} \tag{6}$$

Here, k_2 (g mg^{-1} min^{-1}) is a pseudo-second-order model rate constant. The plot Fig. 7(b) was used to evaluate the parameters of pseudo-second-order adsorption. The value of R^2 obtained for the pseudo-second-order kinetic model is 0.9998, close to unity and higher than the value of R^2 of the pseudo-first-order plot [Fig. 7(b)]. Consequently, it can be inferred that a 99.98% variation in the experimental data of this study is explained more accurately by the pseudo-second-order model. This fitting also

unveils that chemical forces are acting during the process. The values of q_e and k_2 obtained were 3.9873 mg g^{-1} and 0.142 g mg^{-1} min^{-1}, respectively.

To explore the adsorption process, the intraparticle diffusion model was elucidated, which cannot be studied through previously described models. Moreover, the intraparticle diffusion model was fitted to clarify the intraparticle diffusion process if it is the rate-determining step for the overall MB removal by AMD. The intraparticle equation used is as follows (eqn (7)):

$$q_t = k_i t^{\frac{1}{2}} + C_{ip} \tag{7}$$

Here, k_i (g mg^{-1} min$^{-1/2}$) is the rate constant for intraparticle diffusion and C_{ip} is the constant associated with the degree of boundary layer effect, *i.e.*, thickness of the boundary layer and extrinsic mass transfer resistance. The intraparticle model plot [Fig. 7(c)] is demarcated into three segments, *viz.* 1, 2 and 3, which have their own significance. Segment 1 shows film diffusion at the commencement of the process, where the adsorption occurs on the outer surface of AMD with the quick adsorption of a considerable amount of MB. Segment 2 indicates the adsorption of MB on the external surface of pores along with the wall of pores, while segment 3 represents intraparticle diffusion and adsorption in the interior surface of the pores, respectively, where MB molecules are adsorbed into the pores of AMD afterward. During the process, the MB molecules interact and occupy more and more with the adsorption sites of AMD particles and reach an equilibrium stage where the diffusion rate decreases and the amount of MB adsorbed does not increase gradually. The results suggest that the adsorption process for the removal of MB on AMD is not independently governed by intraparticle diffusion as the plot does not pass
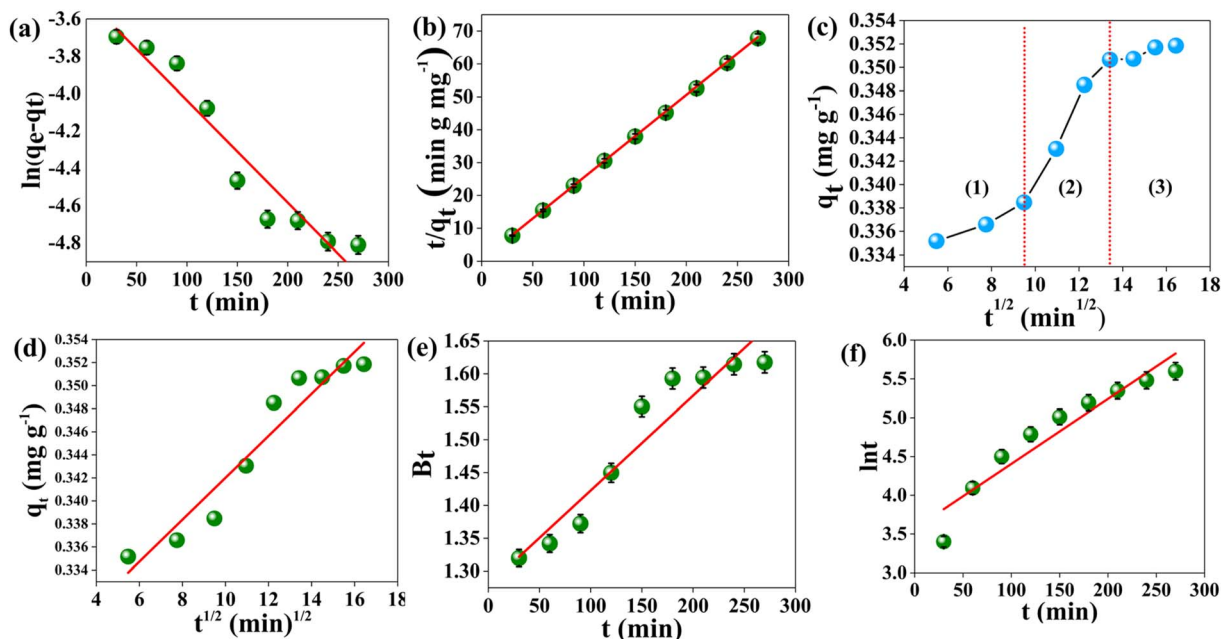

Fig. 7 Kinetic models for MB adsorption on the AMD surface (a) pseudo-first order (b) pseudo-second order (c) intraparticle. (d) Linear fitted intraparticle plot (e) Boyd (f) Elovich [10 mg L^{-1}]. Initial MB concentration at adsorbent dose of 1 g at 313 K at pH 6 for 30–270 min.

through the origin ($C = 0$) [Fig. 7(d)], illustrating the potential participation of additional mechanisms like pore diffusion, film diffusion or surface adsorption.[38,39]

In order to determine the actual rate-determining step for MB removal and distinguish between pore diffusion and external transport (film diffusion), the Boyd kinetic model was applied.

$$F = \frac{q_t}{q_e} = 1 - \left[\left(\frac{6}{\pi^2} \right) \times \sum_{n=1}^{\infty} \frac{1}{n^2} \times e^{-n^2 \times B_t} \right] \qquad (8)$$

In eqn (8), B_t (mathematical function of F) could be calculated as $B_t = -0.4977 - \ln(1 - F)$, where F is the fraction of MB adsorbed after time t, q_e is (mg g^{-1}) the equilibrium adsorption amount and q_t (mg g^{-1}) is the adsorbed amount at time t. If the straight line of a graph plotted between B_t and t (Boyd plot) passes through the origin, then pore diffusion is predominantly the rate-determining step, and if not, then the rate-determining step is film diffusion. Fig. 7(e) displays a straight line not passing through the origin, showing film diffusion as the rate-determining step for MB removal by AMD.[40] This illustrates the potential participation of additional mechanisms like physisorption.[38] All the estimated values are provided in Table 5.

The Elovich model [Fig. 7(f)] could be described by plotting a graph between q_t and $\ln t$ following the below eqn (9):

$$q_t = \frac{1}{\beta} \ln \alpha\beta + \beta \ln t \qquad (9)$$

α (mg g^{-1} min^{-1}) and β (g mg^{-1}) are the initial adsorption rate constant and constant corresponding to the extent of surface coverage and E_a for chemisorption, respectively. The calculated parameters are listed in Table 5.

3.5 Adsorption isotherm

Various mathematical models are known to illustrate the interaction between the adsorbent surface and adsorbate molecules called adsorption isotherms. To study the isotherm of MB adsorption, Langmuir, Freundlich, Temkin and Redlich–

Peterson models were linearly fitted individually to reveal the suitable model. These models facilitate an understanding of the adsorption mechanism and provide insights into the arrangement of adsorption sites on the AMD surface. In this study, adsorption experiments were performed at differing initial MB concentrations of 10, 20, 30 40, 50, 60 and 70 mg L^{-1} and maintaining other variables at 1 g AMD dose for 135 min at 313 K at pH 6.

The Langmuir isotherm (eqn (10)) signifies the formation of a monolayer, while on the contrary, the Freundlich isotherm (eqn (11)) describes the formation of a multi-layer on heterogeneous surfaces. The Langmuir model considers equivalent adsorption sites and constant enthalpy, while the Freundlich model assumes exponential diffusion of adsorption sites and their enthalpy.[41] The Temkin model (eqn (12)) describes adsorption as a function of temperature where the adsorption enthalpy decreases linearly due to an increase in the adsorption surface, consequently due to the interaction of the adsorbate molecules and adsorbent. According to this model, adsorption is described by adsorption binding energies which are homogeneously distributed up to maximum value of binding energy.[42] The Redlich–Peterson isotherm model (R–P model) (eqn (13)) is an amalgamation of Langmuir and Freundlich models, which follows an ideal Langmuir condition at low concentrations when the value of β approaches one and converges to Freundlich when the value of β is nearly zero.

$$\frac{C_e}{q_e} = \frac{C_e}{q_{max}} + \frac{1}{q_{max} K_L} \qquad (10)$$

$$\ln q_e = \ln K_f + \frac{1}{n} \ln C_e \qquad (11)$$

$$q_e = B_T \ln(A_T) + B_T \ln(C_e) \qquad (12)$$

$$\ln \left[\frac{C_e}{q_e} \right] = \beta \ln C_e - \ln k_R \qquad (13)$$

Here, C_e (mg L^{-1}) is the equilibrium MB concentration, q_{max} (mg g^{-1}) is the maximum monolayer adsorption capacity, k_L (L

Table 5 Calculated values for different kinetic models for MB removal by AMD

Kinetic model	Equation	Parameters
Pseudo-first order	$\ln(q_e - q_t) = \ln q_e - k_1 t$	$R^2 = 0.9303$ $K_1 = 0.0054$ min^{-1} $q_e = 0.035$ mg g^{-1}
Pseudo-second order	$\dfrac{t}{q_t} = \dfrac{1}{K_2 q_e^2} + \dfrac{t}{q_e}$	$R^2 = 0.9998$ $q_e = 3.987$ mg g^{-1} $k_2 = 0.142$ g mg^{-1} min^{-1}
Intraparticle	$q_t = k_i t^{\frac{1}{2}} + C_i$	$R^2 = 0.9308$ $k_i = 0.0018$ g mg^{-1} min$^{-1/2}$ $I = 0.3238$
Boyd	$F = \dfrac{q_t}{q_e}$ $F = 1 - \left[\left(\dfrac{6}{\pi^2} \right) \times \sum_{n=1}^{\infty} \dfrac{1}{n^2} \times e^{-n^2 \times B_t} \right]$	$R^2 = 0.9127$
Elovich	$q_t = \dfrac{1}{\beta} \ln \alpha\beta + \beta \ln t$	$R^2 = 0.9118$ $A = 123.223$ mg g^{-1} min^{-1} $B = 0.00836$ g mg^{-1}

mg^{-1}) is the Langmuir constant that signifies the interaction of adsorption sites and their energies, $k_f (\text{mg L}^{-1})$ is the Freundlich constant that indicates the adsorbate–adsorbent relationship, and $1/n$ shows the adsorption capacity and heterogeneity of adsorbent surface. The value of n reveals the adsorption type, *viz.* chemical ($n < 1$), linear ($n = 1$) and physical ($n > 1$).[41] The k_R and β in eqn (13) are Redlich–Peterson constants, while A_T (L g^{-1}) is the binding constant at the equilibrium stage representing the maximum binding energy and B_T (kJ mol^{-1}) is the Temkin constant for adsorption heat.[43] Furthermore, a constant b (J mol^{-1}), *i.e.*, Temkin isotherm constant associated with adsorption heat, is calculated from formula $b = RT/B_T$. Here, T (K) is the temperature and R (8.314 J mol^{-1} K^{-1}) is the universal gas constant.

From Fig. 8, it could be observed that the adsorption of MB on AMD is comparatively more consistent with the Langmuir isotherm model than other isotherm models. Consequently, it can be said that the adsorption process obeys the Langmuir isotherm model ($R^2 = 0.97513$) and MB removal follows monolayer adsorption. The values of q_{max} and K_L are 1.165 mg g^{-1} and 0.227 L g^{-1}, respectively, by plotting a graph between C_e/q_e and $1/q_{max}$ following eqn (8). These values indicate appreciable maximum adsorption capacity and significant interaction between the adsorbent and adsorbate. Additionally, the value of R_L was calculated as 0.305, which indicates favorable adsorption of MB on the AMD surface. The detailed R^2 values of other isotherm models are given in Table 6.

3.6 Adsorption thermodynamics

Thermodynamics plays a pivotal role in investigating the adsorption mechanism and influence of independent variables like temperature. The adsorption experiments were conducted

Table 6 Calculated values of parameters for different isotherm models for MB removal by AMD

Isotherm	Equation	Parameters
Langmuir	$\dfrac{C_e}{q_e} = \dfrac{C_e}{q_{max}} + \dfrac{1}{q_{max}K_L}$	$R^2 = 0.9751$ $q_{max} = 1.165$ mg g^{-1} $R_L = 0.305$ $K_L = 0.227$ L g^{-1}
Freundlich	$\ln q_e = \ln K_f + \dfrac{1}{n}\ln C_e$	$R^2 = 0.9677$ $n = 0.435$ $K_f = 16.395$ mg L^{-1}
Temkin	$q_e = B_T \ln(A_T) + B_T \ln(C_e)$	$R^2 = 0.8843$ $B_T = 3.495$ kJ mol^{-1} $A_T = 0.832$ L gm^{-1} $b = 744.40$ J mol^{-1}
Redlich–Peterson	$\ln\left[\dfrac{C_e}{q_e}\right] = \beta \ln C_e - \ln k_R$	$R^2 = 0.8247$ $k_R = 2.138$ $\beta = 0.717$

at 30 mg L^{-1} initial MB concentration, 1 g AMD dosage for 135 min at pH 6 at varying temperatures (303, 313, 323 K). The thermodynamic parameters were enumerated to examine the dynamics of adsorption. The parameters, *i.e.*, Gibb's free energy ($\Delta G°$), enthalpy ($\Delta H°$), and entropy ($\Delta S°$), were calculated from the van't Hoff equation given below:

$$\Delta G° = -RT \ln K_d \qquad (14)$$

$$\Delta G° = \Delta H - T\Delta S° \qquad (15)$$

From eqn (14) and (15)

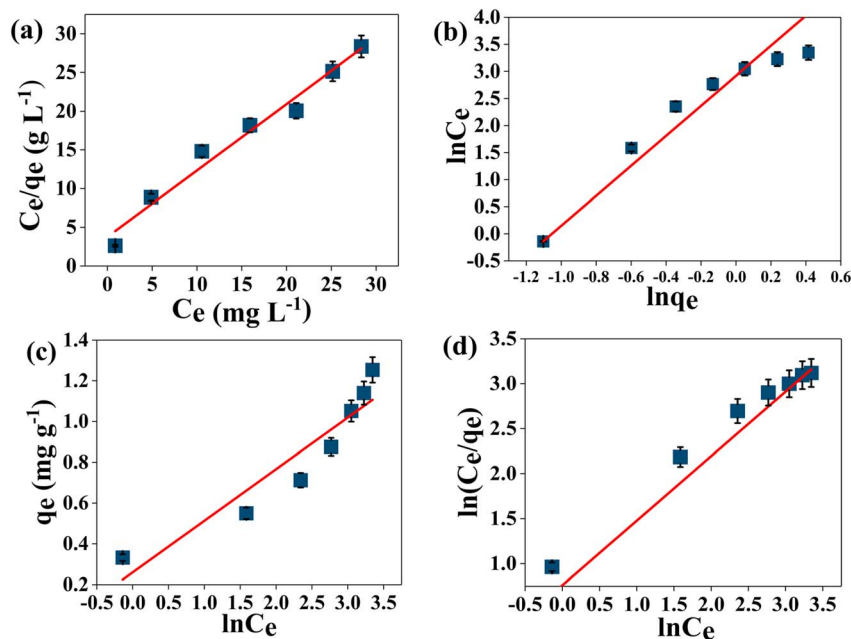$$\ln K_C = \frac{\Delta S°}{R} - \frac{\Delta H°}{RT} \qquad (16)$$

Fig. 8 Adsorption isotherm plots for MB dye removal [initial MB concentration from 10–70 mg L^{-1} at 1 g AMD dose for 135 min at 313 K at pH 6] (a) Langmuir (b) Freundlich (c) Temkin and (d) Redlich–Peterson.

K_C is the thermodynamic equilibrium constant, T (K) is the temperature and R (8.314 J mol^{-1} K^{-1}) is the universal gas constant. The values of ΔH° and ΔS° (eqn (16) estimated from eqn (14) and (15)) were estimated from the slope and intercept of the graph of $\ln K_C$ *vs.* $1/T$, and ΔG° was calculated by Van't Hoff equation (eqn (15)) given in ESI file Fig. S2.† The value of ΔG° is negative for all the temperatures, *viz.* −4.40, −3.74, −3.08 kJ mol^{-1} at 303, 313, 323 K, respectively. The negative magnitude of ΔG° validates a feasible and spontaneous process. Mining in the empirical results, it was unveiled that the values of ΔG° experienced a dip from 303 to 313 K, showing the adsorption process probably has some physical interactions.[44] It was noted from the ΔG° values that the process of MB adsorption on the AMD surface is more favorable at 303 K. The obtained negative value of ΔH° ($\Delta H^\circ = -24.495$ kJ mol^{-1}) shows that the process is exothermic, which signifies that the energy released from the bond formation between adsorbent–adsorbate is greater than the total amount of energy absorbed in bond breaking between the adsorbate and solvent molecules adsorbed previously. It can also be concluded that the MB-AMD interaction is stronger than the preadsorbed solvent. Additionally, the value of ΔH° shows the type of adsorption *viz.* ΔH° value less than 40 kJ suggests physisorption while a value higher than 80 kJ mol^{-1} shows chemisorption. Here, the value of ΔH° is below 40 kJ mol^{-1}, which shows physisorption.[45] The value of ΔH° could also be calculated by plotting a graph between q_e and C_e, *i.e.*, Henry's law (eqn (17)). The Henry's law is applied for very low solute concentrations to allow solute molecules isolate themselves from their neighboring molecules. The value of ΔH° is determined using eqn (17) and (18) as follows:

$$q_e = k_H C_e \tag{17}$$

The ΔH° could be calculated by

$$k_H = k_0 \, e^{-\Delta H/RT} \tag{18}$$

$$\ln k_H = \ln k_0 - \frac{\Delta H}{RT} \tag{19}$$

In this instance, k_H is Henry's constant and k_0 is the mathematical constant. A linear fit graph is plotted between $\ln k_H$ and $1/T$ by following eqn (19), where k_0 and ΔH° were evaluated by the intercept and slope of the graph. Interestingly, the value of ΔH° was found to be −20 kJ mol^{-1}, which is close to its value obtained by eqn (18) verifying exothermic reaction. The plots are given in the ESI file (Fig. S3).† The negative value of ΔS°, *i.e.*, −66.288 J mol^{-1} K^1 shows a high degree of ordering of MB molecules on the AMD interface.[46–48] Moreover, the negative value of ΔS° also signifies no substantial change in the internal structure of the adsorbent during the whole process of adsorption.[49,50] The values of all the thermodynamic parameters are tabulated in Table 7.

Additionally, the physisorption mechanism is supported as the principal mechanism by determining the values of E_a (activation energy) and S^* (sticking probability) from the empirical data (eqn (20)). The adhesion probability depends on the adsorbent/adsorbate and temperature of the investigating

Table 7 Calculated thermodynamic parameters for the removal of MB using AMD [30 mg L^{-1} initial MB concentration, 1 g AMD dosage for 135 min at pH 6 at 303, 313, 323 K temperatures]

Thermodynamic parameters	Methylene blue dye
ΔH° (kJ mol^{-1})	−24.49
ΔS° (J mol^{-1} K^{-1})	−66.288
ΔG° (kJ mol^{-1}) at 303 K	−4.40
313 K	−3.74
323 K	−3.08

system. The S^* value designates the estimation of the capacity of the adsorbate to adsorb on the adsorbent surface indefinitely. These parameters were quantified by the modified Arrhenius-type equation as given below:

$$\ln(1 - \theta) = \ln S^* - \left[\frac{E_a}{R}\right]\frac{1}{T} \tag{20}$$

The value of S^* lying in the range of $0 < S^* < 1$ shows favorable adsorption, while its value $S^* = 1$ indicates the adsorption follows a combination of physical and chemical adsorption and a linear affinity between the adsorbent and adsorbate. Its value $S^* = 0$ depicts indefinite sticking of the adsorbate and adsorbent *via* chemical adsorption and $S^* > 1$ shows no adsorption. For this instance, batch experiments were performed at 10 mg L^{-1} initial dye concentration, pH 6, and 0.55 g AMD dose at 303, 313, 323 K. On plotting the graph $\ln(1 - \theta)$ *versus* $1/T$ (Fig. S2 ESI file),† the values of E_a and S^* of 28.14 kJ mol^{-1} and 2.73×10^{-6} were calculated. The value of S^* confirms favorable adhesion and a high probability of the adsorption of MB on adsorption sites.[44] The negative magnitude of E_a shows the exothermic nature of the process.[51] The value of surface coverage is obtained by eqn (21), where C_e and C_0 are the equilibrium and initial MB concentrations (mg L^{-1}).

$$\theta = 1 - \frac{C_e}{C_0} \tag{21}$$

3.7 Adsorption mechanism

The insights on the surface and chemical state of groups of the adsorbent provide vital information for predicting the adsorption mechanism. The XPS characterization of the adsorbent before and after adsorption was performed by making a pellet of 2 mm. The XPS survey scan before adsorption (Fig. S4 ESI file†) indicates Ca 2p, O 1s, and C 1s peaks with 15.33, 50.99 and 33.68%. Here, it can be noted that a carbon tape was used while conducting the XPS characterization, which shows the presence of C in AMD. The absence of C could also be confirmed by other characterizations mentioned previously. The elemental composition after adsorption shows 13.03, 49.37, 36.24% of Ca 2p, 49.37% O 1 s, and 36.24% C 1s peaks with the appearance of N 1s with 1.37% verifying MB adsorption. The decrease in the atomic percentage of Ca and O with the increase in C content also signifies MB adsorption.

The Ca 2p high-resolution spectra [Fig. 9(a)] show two peaks at 346.58 and 350.08 eV corresponding to Ca 2p$_{1/2}$ and Ca 2p$_{3/2}$. The peak at 346.58 eV could be deconvoluted in two peaks at 346.58 and 346.68 eV, representing the Ca^{2+}, while the peak at 350.08 eV deconvoluted in 350.08 and 350.18 showing the surface Ca element.[52,53] It is noted that the binding energy of the peak at 350.18 eV increases slightly to 350.28 eV after adsorption, indicating Ca in charge balance and its presence outside the skeleton. Additionally, another probable reason for an increase in binding energy is the formation of coordinate bonds between the vacant orbitals of Ca and nucleophilic atoms of the dye, *i.e.*, N. The formation of coordinate bonds leads to an increase in the stability of Ca–O bonds. However, Fig. 9(b) displays the O 1s spectrum with a single peak at 530.98 eV, which is deconvoluted into three peaks at 529.88, 530.98, and 531.68 eV, corresponding to three states of oxygen *viz.* lattice oxygen, O^{2-}/carboxylic oxygen and absorbed oxygen, respectively. Out of these peaks, the peak corresponding to lattice oxygen shifted slightly to 529.78 eV, showing the participation of oxygen moieties during process.[54,55]

A high-resolution scan of N 1s [Fig. 9(c)] was performed for AMD before and after adsorption, where a peak was observed at 399.98 eV after adsorption. This peak was deconvoluted into three peaks at 399.2, 399.98, and 402.3 eV, indicating benzene and –N(CH$_3$)$_2$ groups, N atom in conjugation in the –C=N– group, and the protonated amino group, respectively, confirming the involvement of N of MB in adsorption.[56] The C 1s spectra [Fig. 9(d)] show a doublet at 284.38 and 289.18 eV, representing C–C/C=C and O–C=O, respectively. The peak at 284.37 eV deconvoluted into 284.38 and 285.18 eV, signifying C–O and C–C, C–H and C–N, respectively. The peak at 289.18 eV is the sum of peaks at 287.88 and 289.18 eV, showing C=O and O–C=O of the carboxylic group. It was observed from the C 1s spectrum that peaks were slightly shifted to 284.18 and 289.08 eV, showing the interaction between the oxygen moieties of AMD and –CH$_3$ group of MB by hydrogen bond. It could also be deciphered that the MB diffuses swiftly through the solution to the AMD surface adsorption sites. The formation of coordinate bonds and hydrogen bonds favors the adsorption process.

The MB diffuses to the pores of AMD, which is efficiently improved by microporous filtration to ensure adsorption efficiency till the saturation of adsorption sites of AMD.[57] Thus, the adsorption of MB is ascribed by the formation of hydrogen bonds, covalent bonds and pore filling mechanism (Fig. 10).

3.8 Regeneration studies

In adsorption studies, reusability is a crucial parameter in determining the cost-efficiency and economic feasibility of an adsorbent. Thus, in order to assess this parameter, multiple adsorption–desorption cycles were conducted for AMD. Batch experiments were conducted for 30 mg L^{-1} initial MB concentrations at pH 6 for 1 g AMD dose for 135 min at 313 K. After each cycle, the used AMD was washed with DI (deionized) water multiple times, followed by drying in a hot air oven. The dried AMD was utilized further for the next consecutive cycles. The empirical data indicated promising reusability with five consequent recoveries of 98.11, 94.31, 86.09, 74.09, and 62.35%, respectively. The detailed examination of the study reveals that there is a slight decline in the removal efficiency after multiple cycles. Therefore, the AMD adsorbent emerges and proves to be an inexpensive, sustainable, and durable adsorbent with rapid efficiency in MB dye removal [ESI file Fig. S5†].

3.9 Comparative study with the reported adsorbents

As reported in previous studies, research has been done on diverse adsorbents for the removal of MB. The competitiveness of AMD with reported adsorbents was investigated, as listed in Table 8. It could be elucidated that the adsorbent used in the present study has reasonable removal efficiency and a strong affinity for the removal of MB. All the studies involve the use of CCD RSM in their studies.

The advantage of using RSM is that its results minimize the complexities of the process, providing insights into the effects
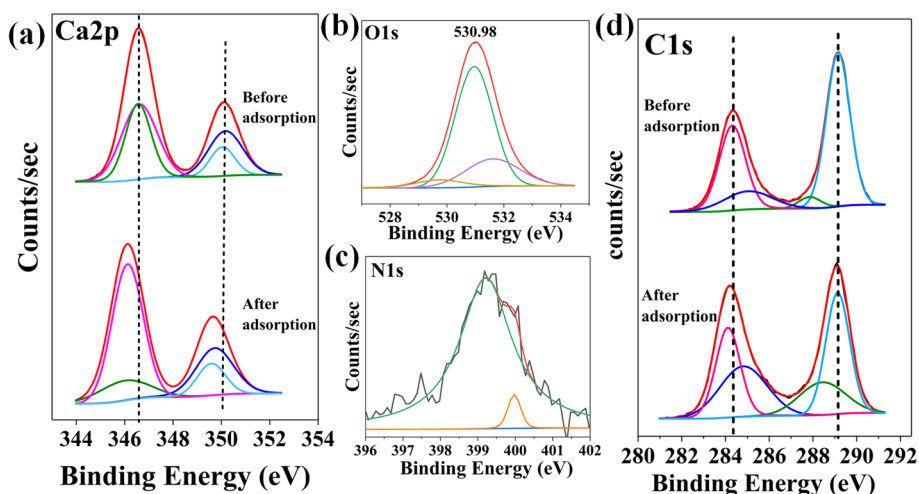

Fig. 9 XPS results indicating (a) Ca 2p spectra before and after adsorption (b) O 1s spectra after adsorption (c) N 1s spectra after adsorption (d) C 1s spectra before and after adsorption.
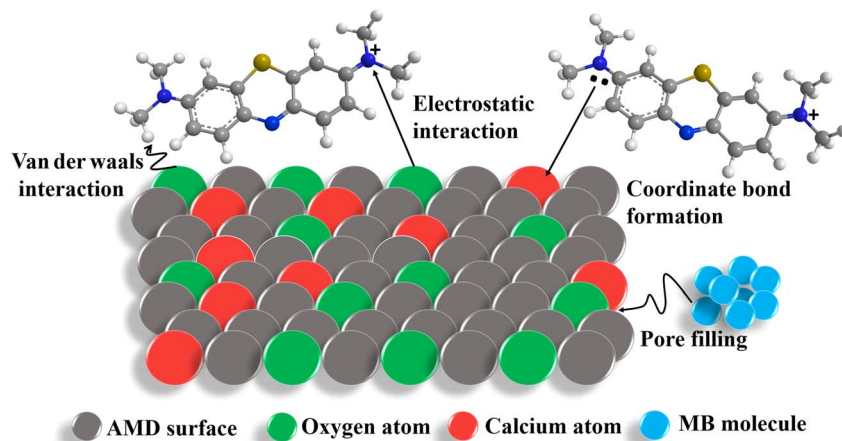
Fig. 10 Potential adsorption mechanism of MB adsorption on AMD.

Table 8 A comparison of previous studies of low-cost adsorbents for MB adsorption

Adsorbent	Method of preparation	Variables studied	MB removal (%) and q_{max}	Reference
Nano-zero valent iron	Liquid phase reduction	pH, time, adsorbent dose, initial MB concentration	92.21% —	58
Activated carbon from *N. microphyllum*	Nitrogen inert atmosphere	pH, time, adsorbent dose, initial MB concentration	97% —	59
Biosorbent walnut shells (*Juglans regia*)	Pulverization	pH, time, adsorbent dose, initial MB concentration	97.74% —	60
Thermally activated kaolinite	Annealing	pH, time, adsorbent dose, initial MB concentration, size of particles	90% 97.8 mg g^{-1}	61
Ho-CaWO$_4$	Hydrothermal method	pH, initial MB concentration, time, adsorbent dose	71.17% 103.09 mg g^{-1}	62
Bi-functionalized xerogel		pH, time, initial MB concentration	99.8% 512 mg g^{-1}	63
Chemically modified porous carbon	Pyrolysis	pH, initial MB concentration, adsorbent dose	90% 181.82 mg g^{-1}	64
Elaeis guineensis-biochar activated by ZnCl$_2$	Thermochemical activation with ZnCl$_2$	Particle size, time, temperature	93.2% 48.8 mg g^{-1}	65
Activated marble dust	Pulverization and annealing	pH, time, temperature, adsorbent dose, initial MB concentration	96.76% q_{max} = 1.16 mg g^{-1}	Present study

of interactions between variables. These results provide a blue-print for the optimization process to achieve the maximum removal of dyes. Therefore, the advantages of AMD, such as simplicity, inexpensive, novel, sustainable, easy, and large-scale availability, make it commending for industrial use.

4 Conclusion

The impact of research work on society is from its simplicity, applicability, and cost-efficiency. The investigation of this article provides insight into utilizing metallurgical waste as a facile, economical, sustainable and industrially applicable adsorbent. The preparation method of the adsorbent is facile and analyzed through thorough mechanistic studies like XRD,

BET, TGA, FE-SEM, and FTIR, followed by utilization in the removal of MB dye. The interactive and combined effects of different variables, such as temperature, pH, and amount of AMD, were investigated using the CCD model of RSM with a justified R^2 value of 0.9914. The ANOVA results, including the lack of fit and *p*-value, also verify the quadratic model. The 3D response plots provide clarity on the influence of variables on the removal percentage. The pH of the system greatly influenced the removal yield of MB. The removal followed pseudo-second order kinetics (R^2 = 0.999) and Langmuir isotherm model (R^2 = 0.9751) of monolayer adsorption with q_{max} = 1.16 mg g^{-1}. A potential mechanism of dye removal was studied *via* XPS analysis. To explore the energetics of the process, a thermodynamic study was conducted, which revealed the adsorption of MB is

exothermic and spontaneous where the process falls under Henry's law region and unveils that the removal of MB is feasible in terms of reproducibility up to five cycles. Therefore, the marble dust could provide a sustainable and low-cost adsorbent with wide applications in water treatment in low- and middle-income nations.

Consent for publication

All the authors consented to the publication of this research article.

Data availability

The data supporting this article have been included as a part of the ESI.†

Author contributions

Ankita Sharma: methodology; investigation; data collection; formal analysis; writing original draft. Subrata Panda: formal analysis; supervision. Sudesh Kumar: formal analysis; supervision. Yogesh Chandra Sharma: conceptualization; methodology, resources; formal analysis, review and editing, supervision. All the authors have read and approved the final manuscript.

Conflicts of interest

The authors declare that they have no competing financial or personal interests that could have potentially influenced the work presented in this study.

Acknowledgements

References

1 E. Tugrul Tunc, *J. Environ. Manage.*, 2019, **231**, 86–97.

2 Q. Iqbal, M. A. Musarat, N. Ullah, W. S. Alaloul, M. B. A. Rabbani, W. Al Madhoun and S. Iqbal, Marble Dust Effect on the Air Quality: An Environmental Assessment Approach, *Sustainability*, 2022, **14**(7), 3831.

3 Y. Saini, N. Bhardwaj and R. Gautum, Effect of marble dust on plants around Vishwakarma Industrial Area (VKIA) in Jaipur, India. Journal of Environmental Biology, *J. Environ. Biol.*, 2011, **32**, 209–212.

4 I. Khan, I. Khan, M. Usman, M. Imran and K. Saeed, Nanoclay-mediated photocatalytic activity enhancement of copper oxide nanoparticles for enhanced methyl orange photodegradation, *J. Mater. Sci.: Mater. Electron.*, 2020, **31**, 8971–8985.

5 Y. C. Sharma, Uma and S. N. Upadhyay, Removal of a cationic dye from wastewaters by adsorption on activated carbon developed from coconut coir, *Energy Fuels*, 2009, **23**, 2983–2988.

6 G. S. Singhal and E. Rabinowitch, Changes in the absorption spectrum of methylene blue with pH, *J. Phys. Chem.*, 1967, **71**, 3347–3349.

7 M. M. Brooks, Methylene blue as antidote for cyanide and carbon monoxide poisoning, *J. Am. Med. Assoc.*, 1933, **100**, 59.

8 H. N. Hamad and S. Idrus, *Polymers*, 2022, **14**, 783.

9 H. I. Kelle, E. C. Ogoko, O. Akintola and N. O. Eddy, Quantum and experimental studies on the adsorption efficiency of oyster shell–based CaO nanoparticles (CaONPO) towards the removal of methylene blue dye (MBD) from aqueous solution, *Biomass Convers. Biorefin.*, 2023, **14**, 31925–31948.

10 A. Asghar, A. A. A. Raman and W. M. A. W. Daud, *J. Cleaner Prod.*, 2015, **87**, 826–838.

11 Y. C. Sharma, Adsorption characteristics of a low-cost activated carbon for the reclamation of colored effluents containing malachite green, *J. Chem. Eng. Data*, 2011, **56**(3), 478–484.

12 M. Liu, Q. Chen, K. Lu, W. Huang, Z. Lü, C. Zhou, S. Yu and C. Gao, High efficient removal of dyes from aqueous solution through nanofiltration using diethanolamine-modified polyamide thin-film composite membrane, *Sep. Purif. Technol.*, 2017, **173**, 135–143.

13 M. Liu, Y. Guo, J. Lan, Y. Zhou, Q. Dong and C. Guo, Synthesis of Ce/SiO2 Composited Cross-Linked Chitosan Flocculation Material and Its Application in Decolorization of Tartrazine Dye, *ChemistrySelect*, 2019, **4**, 13156–13162.

14 A. Rafiq, M. Ikram, S. Ali, F. Niaz, M. Khan, Q. Khan and M. Maqbool, *J. Ind. Eng. Chem.*, 2021, **97**, 111–128.

15 V. Srivastava, Y. C. Sharma and M. Sillanpää, Response surface methodological approach for the optimization of adsorption process in the removal of Cr (VI) ions by $Cu_2(OH)_2CO_3$ nanoparticles, *Appl. Surf. Sci.*, 2015, **326**, 257–270.

16 D. Gusain, F. Bux and Y. C. Sharma, Abatement of chromium by adsorption on nanocrystalline zirconia using response surface methodology, *J. Mol. Liq.*, 2014, **197**, 131–141.

17 R. Shu, J. Bai, F. Guo, S. Mao, Q. Qiao, K. Dong, L. Qian and Y. Bai, Synthesis of carbon/P-zeolite composites from coal gasification fine slag and studies on adsorption characteristics for methylene blue, *Korean J. Chem. Eng.*, 2023, **40**, 1639–1649.

18 N. A. M. Barakat, H. A. Omran, M. K. Hassan, A. F. Mohamed, A. H. Backar, O. M. Irfan and O. A. Mohamed, Graphite-TiO2-doped coated sand granules for efficient continuous removal of methylene blue dye: Combining adsorption and photocatalytic degradation, *Results Eng.*, 2023, **20**, 101646.

19 A. S. Elkholy, M. S. Yahia, M. A. Elnwawy, H. A. Gomaa and A. S. Elzaref, Synthesis of activated carbon composited with

Egyptian black sand for enhanced adsorption performance toward methylene blue dye, *Sci. Rep.*, 2023, **13**, 4209.

20 M. M. Hamed, I. M. Ahmed and S. S. Metwally, Adsorptive removal of methylene blue as organic pollutant by marble dust as eco-friendly sorbent, *J. Ind. Eng. Chem.*, 2014, **20**, 2370–2377.

21 B. N. Shelke, M. K. Jopale and A. H. Kategaonkar, *J. Indian Chem. Soc.*, 2022, **99**, 100530.

22 J. Cheng, C. Bi, X. Zhou, D. Wu, D. Wang, C. Liu and Z. Cao, Preparation of Bamboo-Based Activated Carbon via Steam Activation for Efficient Methylene Blue Dye Adsorption: Modeling and Mechanism Studies, *Langmuir*, 2023, **39**, 14119–14129.

23 G. A. Lujan-Moreno, P. R. Howard, O. G. Rojas and D. C. Montgomery, Design of experiments and response surface methodology to tune machine learning hyperparameters, with a random forest case-study, *Expert Syst. Appl.*, 2018, **109**, 195–205.

24 A. Jahan, K. L. Edwards and M. Bahraminasab, in *Multiple objective decision-making for material and geometry design*, 2016, pp. 127–146.

25 S. Akazdam, S. Kaba, M. Chafi, L. H. Omari and H. Hiyane, Removal of Acid orange 7 dye in continuous fixed-bed reactor by alkaline treated eggshell: experimental and numerical modeling, *Desalination Water Treat.*, 2022, **268**, 89–98.

26 A. Pappu, R. Chaturvedi and P. Tyagi, Sustainable approach towards utilizing Makrana marble waste for making water resistant green composite materials, *SN Appl. Sci.*, 2020, **2**, 347.

27 B. J. Zhan, D. X. Xuan, C. S. Poon, C. J. Shi and S. C. Kou, Characterization of C–S–H formed in coupled CO2–water cured Portland cement pastes, *Mater. Struct.*, 2018, **51**, 92.

28 V. Singh Kashyap, U. Agrawal, K. Arora and G. Sancheti, in *IOP Conference Series: Earth and Environmental Science*, IOP Publishing Ltd, 2021, vol. 796.

29 A. K. Jain, A. K. Jha and Shivanshi, Geotechnical behaviour and micro-analyses of expansive soil amended with marble dust, *Soils Found.*, 2020, **60**, 737–751.

30 A. I. Hussein, Z. Ab-Ghani, A. N. C. Mat, N. A. A. Ghani, A. Husein and I. A. Rahman, Synthesis and characterization of spherical calcium carbonate nanoparticles derived from cockle shells, *Appl. Sci.*, 2020, **10**, 1–14.

31 R. O. Gembo, S. Odisitse, T. A. M. Msagati and C. K. King'ondu, The beneficiation of asphalt waste through conversion into an efficient activated carbon adsorbent for diazinon pesticide, optimized through response surface methodology, *RSC Sustainability*, 2024, **2**, 2026–2042.

32 J. Cheng, C. Bi, X. Zhou, D. Wu, D. Wang, C. Liu and Z. Cao, Preparation of Bamboo-Based Activated Carbon via Steam Activation for Efficient Methylene Blue Dye Adsorption: Modeling and Mechanism Studies, *Langmuir*, 2023, **39**, 14119–14129.

33 H. Bassareh, M. Karamzadeh and S. Movahedirad, Synthesis and characterization of cost-effective and high-efficiency biochar for the adsorption of Pb2+ from wastewater, *Sci. Rep.*, 2023, **13**(1), 15608.

34 N. Mansouriieh, M. R. Sohrabi and M. Khosravi, Adsorption kinetics and thermodynamics of organophosphorus profenofos pesticide onto Fe/Ni bimetallic nanoparticles, *Int. J. Environ. Sci. Technol.*, 2016, **13**, 1393–1404.

35 A. Zaman, A. Ghosh, B. Gangopadhyay, J. T. Orasugh, S. Santra, J. Chakrobarty, S. Karmakar, P. Banerjee, S. S. Ray and D. Chattopadhyay, Sustainable Conversion of Waste Carbon Brush and Fly Ash into a Novel Nanocomposite for Selective Adsorption of Cationic Dyes, *ACS Sustainable Resour. Manage.*, 2024, **1**, 978–993.

36 D. Allouss, Y. Essamlali, O. Amadine, A. Chakir and M. Zahouily, Response surface methodology for optimization of methylene blue adsorption onto carboxymethyl cellulose-based hydrogel beads: Adsorption kinetics, isotherm, thermodynamics and reusability studies, *RSC Adv.*, 2019, **9**, 37858–37869.

37 Y. S. Ho and G. Mckay, Pseudo-second order model for sorption processes, *Process Biochem.*, 1999, **34**, 451–465.

38 Dr Saruchi, M. Sharma, M. R. Hatshan, V. Kumar and A. Rana, Sequestration of Eosin Dye by Magnesium (II)-Doped Zinc Oxide Nanoparticles: Its Kinetic, Isotherm, and Thermodynamic Studies, *J. Chem. Eng. Data*, 2021, **66**, 646–657.

39 C. Chen, S. Mi, D. Lao, P. Shi, Z. Tong, Z. Li and H. Hu, Single-step synthesis of eucalyptus sawdust magnetic activated carbon and its adsorption behavior for methylene blue, *RSC Adv.*, 2019, **9**, 22248–22262.

40 P. Sharma and M. R. Das, Removal of a cationic dye from aqueous solution using graphene oxide nanosheets: Investigation of adsorption parameters, *J. Chem. Eng. Data*, 2013, **58**, 151–158.

41 M. Hamdi Karaoğlu, M. Doğan and M. Alkan, Removal of cationic dyes by kaolinite, *Microporous Mesoporous Mater.*, 2009, **122**, 20–27.

42 N. Genli, S. Kutluay, O. Baytar and Ö. Şahin, Preparation and characterization of activated carbon from hydrochar by hydrothermal carbonization of chickpea stem: an application in methylene blue removal by RSM optimization, *Int. J. Phytorem.*, 2022, **24**, 88–100.

43 E. Bulut, M. Özacar and I. A. Şengil, Equilibrium and kinetic data and process design for adsorption of Congo Red onto bentonite, *J. Hazard. Mater.*, 2008, **154**, 613–622.

44 F. Borousan, F. Yousefi and M. Ghaedi, Removal of Malachite Green Dye Using IRMOF-3-MWCNT-OH-Pd-NPs as a Novel Adsorbent: Kinetic, Isotherm, and Thermodynamic Studies, *J. Chem. Eng. Data*, 2019, **64**, 4801–4814.

45 X. Zhao, S. Liu, Z. Tang, H. Niu, Y. Cai, W. Meng, F. Wu and J. P. Giesy, Synthesis of magnetic metal-organic framework (MOF) for efficient removal of organic dyes from water, *Sci. Rep.*, 2015, **5**, 11849.

46 S. Kalam, S. A. Abu-Khamsin, M. S. Kamal and S. Patil, *ACS Omega*, 2021, **6**, 32342–32348.

47 J. S. Piccin, L. A. Feris, M. Cooper and M. Gutterres, Dye adsorption by leather waste: Mechanism diffusion, nature

studies, and thermodynamic data, *J. Chem. Eng. Data*, 2013, **58**, 873–882.

48 S. P. D. Monte Blanco, F. B. Scheufele, A. N. Módenes, F. R. Espinoza-Quiñones, P. Marin, A. D. Kroumov and C. E. Borba, Kinetic, equilibrium and thermodynamic phenomenological modeling of reactive dye adsorption onto polymeric adsorbent, *Chem. Eng. J.*, 2017, **307**, 466–475.

49 X. Hou, G. Zhao and M. Li, Unary Adsorption Isotherms of 2,3,3,3-Tetrafluoropropene on Activated Carbon, *J. Chem. Eng. Data*, 2022, **67**, 1715–1722.

50 T. Mizutani, *Thermodynamics*, Intech, Rijeka, Croatia, 2016.

51 N. K. Amin, Removal of direct blue-106 dye from aqueous solution using new activated carbons developed from pomegranate peel: Adsorption equilibrium and kinetics, *J. Hazard. Mater.*, 2009, **165**, 52–62.

52 K. Saini, A. Kumari, A. Sahoo, K. K. Pant and T. Bhaskar, Eggshell-Lignin Carbon Composite for Methyl Orange Removal from Wastewater, *Ind. Eng. Chem. Res.*, 2023, **62**, 15499–15510.

53 M. Bin Mobarak, N. S. Pinky, F. Chowdhury, M. S. Hossain, M. Mahmud, M. S. Quddus, S. A. Jahan and S. Ahmed, Environmental remediation by hydroxyapatite: Solid state synthesis utilizing waste chicken eggshell and adsorption experiment with Congo red dye, *J. Saudi Chem. Soc.*, 2023, **27(5)**, 101690.

54 I. da S. V. Marques, N. C. da Cruz, R. Landers, J. C.-C. Yuan, M. F. Mesquita, C. Sukotjo, M. T. Mathew and V. A. R. Barão, Incorporation of Ca, P, and Si on bioactive coatings produced by plasma electrolytic oxidation: The role of electrolyte concentration and treatment duration, *Biointerphases*, 2015, 041002, DOI: 10.1116/1.4932579.

55 N. Zhang, H. Xue and R. Hu, The activity and stability of CeO2@CaO catalysts for the production of biodiesel, *RSC Adv.*, 2018, **8**, 32922–32929.

56 P. Chen, Z. fang Cao, X. Wen, J. Wang, F. Yang, P. Qiu, Y. jun Yue, G. yi Liu, S. Wang and H. Zhong, A novel mesoporous silicate material (MS) preparation from dolomite and enhancing methylene blue removal by electronic induction, *J. Taiwan Inst. Chem. Eng.*, 2017, **80**, 128–136.

57 T. Wu, G. Yang, J. Cao, Z. Xu and X. Jiang, Activation and adsorption mechanisms of methylene blue removal by porous biochar adsorbent derived from eggshell membrane, *Chem. Eng. Res. Des.*, 2022, **188**, 330–341.

58 M. Khosravi and S. Arabi, Application of response surface methodology (RSM) for the removal of methylene blue dye from water by nano zero-valent iron (NZVI), *Water Sci. Technol.*, 2016, **74**, 343–352.

59 S. Alireza Mousavi, M. Amin Mehralian and M. Khashij, Methylene blue removal from aqueous solutions by activated carbon prepared from *N. Microphyllum* (AC-NM): RSM analysis, isotherms and kinetic studies, *Global NEST J.*, 2017, **19**, 697–705.

60 S. Kumari, V. D. Rajput, T. Minkina, P. Rajput, P. Sharma, A. K. Verma, S. Agarwal and M. C. Garg, Application of RSM for Bioremoval of Methylene Blue Dye from Industrial Wastewater onto Sustainable Walnut Shell (Juglans regia) Biomass, *Water*, 2022, 3651, DOI: 10.3390/w14223651.

61 J. Karuppaiyan, R. Jeyalakshmi, S. Kiruthika, M. A. Wadaan, M. F. Khan and W. Kim, A study on the role of surface functional groups of metakaolin in the removal of methylene blue: Characterization, kinetics, modeling and RSM optimization, *Environ. Res.*, 2023, 115604, DOI: 10.1016/j.envres.2023.115604.

62 C. A. Igwegbe, L. Mohmmadi, S. Ahmadi, A. Rahdar, D. Khadkhodaiy, R. Dehghani and S. Rahdar, Modeling of adsorption of Methylene Blue dye on Ho-CaWO4 nanoparticles using Response Surface Methodology (RSM) and Artificial Neural Network (ANN) techniques, *MethodsX*, 2019, **6**, 1779–1797.

63 Y. Hannachi and A. Hafidh, Preparation and characterization of novel bi-functionalized xerogel for removal of methylene blue and lead ions from aqueous solution in batch and fixed-bed modes: RSM optimization, kinetic and equilibrium studies, *J. Saudi Chem. Soc.*, 2020, **24**, 505–519.

64 T. Van Tran, L. X. Nong, H. T. T. Nguyen, V. H. Nguyen, D. T. C. Nguyen, T. T. Nguyen, P. Q. Trang, D. H. Nguyen and T. D. Nguyen, Response surface methodology modeling for methylene blue removal by chemically modified porous carbon: Adsorption mechanism and role of surface functional groups, *Sep. Sci. Technol.*, 2021, **56**, 2232–2242.

65 L. K. F. Araújo, A. A. Albuquerque, W. C. O. Ramos, A. T. Santos, S. H. V. Carvalho, J. I. Soletti and M. D. Bispo, Elaeis guineensis-activated carbon for methylene blue removal: adsorption capacity and optimization using CCD-RSM, *Environ. Dev. Sustain.*, 2021, **23**, 11732–11750.